# **Inorganic Chemistry**

pubs.acs.org/IC Article

# Enhanced Deep-Red Phosphorescence in Cyclometalated Iridium Complexes with Quinoline-Based Ancillary Ligands

Sungwon Yoon, Thomas G. Gray, and Thomas S. Teets\*



Cite This: Inorg. Chem. 2023, 62, 7898-7905



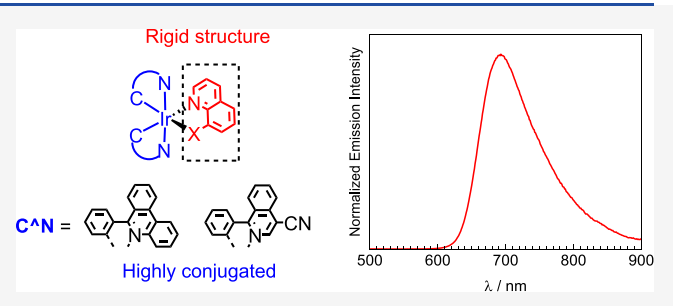
**ACCESS** I

Metrics & More

Article Recommendations

Supporting Information

**ABSTRACT:** Compounds with good photoluminescence quantum yields  $(\Phi_{PL})$  in the deep-red to near-infrared parts of the spectrum are desired for a variety of applications in optoelectronics, imaging, and sensing. However, in this region of the spectrum, quantum yields are usually modest, which is explained by the energy gap law and the inherently slower radiative decay rates for low-energy emitters according to the second-order perturbation theory. In this work, we outline a new direction in deep-red luminescence, introducing a new suite of bis-cyclometalated iridium complexes with efficient luminescence beyond 650 nm.



Seven new complexes are prepared using two different cyclometalating (C^N) ligands with four quinoline-derived ancillary ligands (L^X). The chosen cyclometalating ligands are well-established to produce deep-red phosphorescence and include a metalated phenyl ring appended to a conjugated heterocycle. The ancillary ligands combine a rigid quinoline or benzoquinoline "L" donor with a variable anionic "X" donor comprised of an O-donor aryloxy or carboxylate or an N-donor amidate. These complexes phosphoresce in the deep-red region with wavelengths between 650 and 700 nm and solution quantum yields between 0.018 and 0.42.

### **■ INTRODUCTION**

Cyclometalated iridium(III) complexes are a well-investigated class of molecular phosphors, with a broad range of applications including light-driven catalysis, <sup>1,2</sup> solar electricity, <sup>3,4</sup> solar fuels, <sup>5</sup> and small-molecule sensing. <sup>6,7</sup> Since their explosion onto the scene in the context of electroluminescent color displays, <sup>8</sup> much research has focused on the discovery of cyclometalated iridium complexes with a variety of luminescence color profiles that span the entire visible range. Although deep-red to NIR-emitting (DR-NIR) materials are not necessary for color display applications, there is a growing interest in complementary applications, which require phosphorescence in these regions. <sup>9–11</sup> Besides iridium, complexes with ruthenium, <sup>12–14</sup> osmium, <sup>15–17</sup> platinum, <sup>18–23</sup> and chromium<sup>24–26</sup> can be very efficient for phosphorescence in the red region or even longer wavelengths.

There is a fundamental challenge of designing DR-NIR phosphorescent materials with high photoluminescence quantum yields  $(\Phi_{\rm PL})^{.27}$  In the red region (ca. 600–650 nm), cyclometalated iridium compounds often exhibit a  $\Phi_{\rm PL}$  of ~0.5 in solution,  $^{28-30}$  but extending to DR-NIR, the quantum yields are rarely greater than 0.2.  $^{31-33}$  The quantum yield is dictated by the radiative rate constant  $(k_{\rm r})$  and the nonradiative rate constant  $(k_{\rm nr})$ , more specifically the ratio  $k_{\rm r}/(k_{\rm r}+k_{\rm nr})$ . In these low-energy emitters,  $k_{\rm nr}$  increases on account of the energy gap law,  $^{34-36}$  which is related to the vibrational overlap between the triplet excited state and singlet ground state, whereas  $k_{\rm r}$  is normally lower due to the cubic dependence of  $k_{\rm r}$  on the energy

gap between the ground state and the excited state.<sup>37</sup> The radiative rate constant  $k_r$  is also influenced by excited-state spin-orbit coupling (SOC), which in cyclometalated iridium complexes is dominated by the metal-to-ligand charge transfer (<sup>3</sup>MLCT) states that mix into the phosphorescent triplet state,  $T_1$ . In heteroleptic cyclometalated iridium complexes, the degree of MLCT character in the excited state is responsive to changes in the ancillary ligand(s), so synthetic strategies can be used to increase the MLCT character, which in turn improve  $k_r$  and the quantum yield.

Our group has previously outlined strategies to obtain efficient red to NIR ( $\lambda_{\rm em} > 600$  nm) phosphorescent complexes. <sup>38,39</sup> Incorporating nitrogen-containing, electronrich  $\pi$ -donating ancillary ligands can destabilize the metal-centered HOMO and increase the contribution of the Ir 5d orbitals to the excited state, leading to augmented  $k_{\rm r}$  and  $\Phi_{\rm PL}$  values. This strategy has produced compounds with  $\Phi_{\rm PL}$  values as high 0.8 in the red region <sup>40</sup> and 0.5 in the DR-NIR region when 1-phenylisoquinoline (piq) and substituted analogues are used as the cyclometalating (C^N) ligands. <sup>39,41</sup> In the course of

Received: February 28, 2023 Published: May 11, 2023





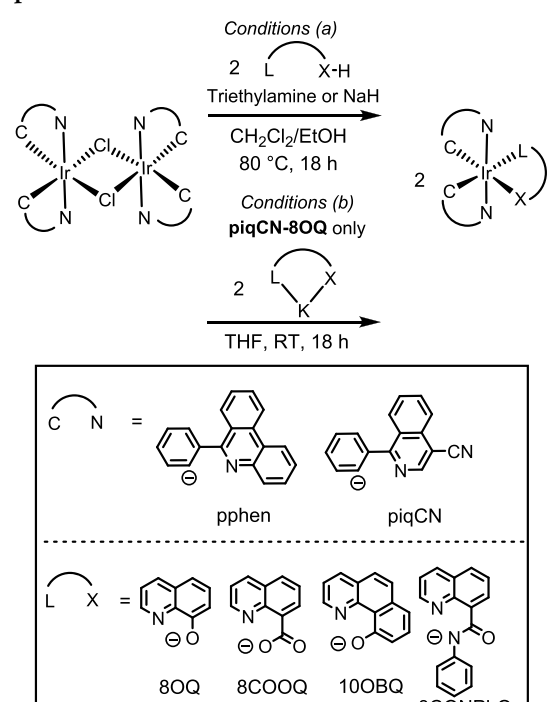
these previous efforts, we found that the effectiveness of electron-rich ancillary ligands depends on the nature of the C^N ligands. In general, complexes with the electron-rich thiophene-based C^N ligands have photoluminescence properties that vary little as the ancillary ligand is changed, but when C^N ligands have simple phenyl rings that metalate, the phosphorescence profile and radiative rate constants depend considerably on the ancillary ligand. 40,42

In this work, we combine these insights to develop a complementary strategy for deep-red bis-cyclometalated iridium complexes with high  $\Phi_{\text{PL}}$  values. The cyclometalating ligands include a N-heterocycle with extended  $\pi$ -conjugation or an electron-withdrawing substituent in order to shift the emission wavelength deeper into the DR-NIR region.<sup>32</sup> Moreover, the C^N ligands are cyclometalated through a phenyl group, which will generate an excited state with substantial <sup>3</sup>MLCT character that will be responsive to the ancillary ligand's electronic characteristics. The ancillary ligands include a quinoline or benzoquinoline neutral donor, which we hypothesized would rigidify the complex and reduce the  $k_{
m nr}$  values, and are substituted with variable electron-rich anionic donor groups that we proposed would modulate the HOMO energy and  $k_r$ . We have previously used these ancillary ligands in the design of DR-NIR phosphors, but our initial investigation yielded photoluminescence properties that were minimally responsive to the ancillary ligand structure. 42 Here, a major goal is to evaluate the effects of these quinoline-derived ancillary ligands on excited states that are more sensitive to the ancillary ligand donor strength and the degree of <sup>3</sup>MLCT character. A total of seven new compounds are introduced in this paper, all of which emit in the deep-red region. The effects of the quinoline-based ancillary ligands and cyclometalating ligands on the frontier orbital energies are evaluated through cyclic voltammetry, complemented with DFT calculations, and detailed photophysical characterization in solution reveals that the excitedstate dynamics and PL wavelengths are responsive to the identity of the anionic donor on the quinoline ancillary ligand.

# ■ RESULTS AND DISCUSSION

Synthesis and Structural Characterization. The syntheses of the seven new complexes with the general formula  $Ir(C^N)_2(L^X)$  (C^N = 6-phenylphenanthridine (pphen) and 1-phenylisoquinoline-4-carbonitrile (piqCN)) are outlined in Scheme 1. The two cyclometalating ligands are known to produce complexes with emission near or beyond 650 nm through extended  $\pi$ -conjugation (pphen) or an added electronwithdrawing group (piqCN) off of the 1-phenylisoquinoline (piq) framework.<sup>28</sup> The two C^N ligands are combined with four quinoline-derived ancillary ligands (L^X) to produce the seven complexes. To abbreviate the structures more concisely, the "C^N-L^X" formalism is used, where C^N indicates the cyclometalating ligand and L^X indicates the ancillary ligand, as defined in Scheme 1. In all cases except piqCN-8OQ, the dimer  $[Ir(C^N)_2(\mu-Cl)]_2$  was heated under reflux with the protonated (neutral) ancillary ligand in mixed CH<sub>2</sub>Cl<sub>2</sub>/ethanol solvent with triethylamine or sodium hydride as the base, conditions we have previously employed for related compounds.<sup>42</sup> To prepare the complex  $piqCN-8OQ_1$  [Ir( $piqCN)_2(\mu-Cl)$ ]<sub>2</sub> was combined with the potassium salt of 8-hydroxyquinoline (8OQK) in tetrahydrofuran at room temperature. Attempted syntheses of piqCN-10OBQ resulted in a poorly defined mixture of products that could not be separated, so that is the one member of the series that is not included in this study. The seven remaining

Scheme 1. Synthesis of the Bis-cyclometalated Iridium(III) Complexes



Compounds studied
pphen-8OQ, pphen-8COOQ, pphen-10OBQ, pphen-8CONPhQ
piqCN-8OQ, piqCN-8COOQ, piqCN-8CONPhQ

complexes were obtained after purification primarily by recrystallization or, in the case of **pphen-8CONPhQ**, column chromatography. Isolated yields ranged between 21 and 50%. The complexes are sparingly soluble, precluding <sup>13</sup>C{<sup>1</sup>H} NMR characterization, but their identity and purity were confirmed by <sup>1</sup>H NMR spectroscopy (Figures S19—S25 of the Supporting Information) and high-resolution mass spectrometry (see the Experimental Section).

**Electrochemistry.** The redox potentials of all complexes were measured by cyclic voltammetry (CV) in THF or  $CH_2Cl_2$  solution. Full CV traces are shown in Figure S1, with the recorded potentials summarized graphically in Figure 1 and numerically in Table 1. The typical electronic structures of bis-

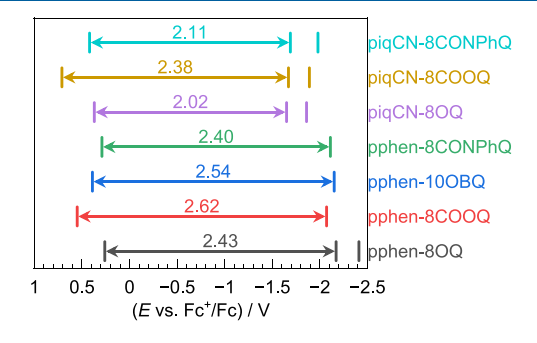


**Figure 1.** Summary of redox potentials determined from cyclic voltammetry experiments. The  $E_{\rm ox}$  values (positive potentials) and  $E_{\rm red}$  values (negative potentials) are plotted, along with a line segment and numerical value that represent the electrochemical HOMO–LUMO gap ( $\Delta E_{\rm H-L}$ ), determined from the difference between  $E_{\rm ox}$  and  $E_{\rm red}$ .

Table 1. Cyclic Voltammetry Data for the Iridium Complexes

	$(E \text{ vs } Fc^+/F$		
complex	$E_{ m red}$	$E_{\text{ox}}$	$\Delta E_{\mathrm{H-L}}^{}}}\left(\mathrm{eV}\right)$
pphen-8OQ	-2.17, -2.41	+0.26 <sup>a</sup>	2.43
pphen-8COOQ	-2.07	+0.55	2.62
pphen-10OBQ	$-2.15^{a}$	+0.39	2.54
pphen-8CONPhQ	-2.11	+0.29	2.40
piqCN-8OQ	-1.65, -1.86	+0.37 <sup>a</sup>	2.02
piqCN-8COOQ	-1.67, -1.89	+0.71 <sup>a</sup>	2.38
piqCN-8CONPhQ	-1.69, -1.98	+0.42 <sup>a</sup>	2.11

<sup>a</sup>Irreversible wave. The half-peak potential is reported. <sup>b</sup>Electrochemical HOMO–LUMO gap, estimated as  $E_{\rm ox}-E_{\rm red}$ .

cyclometalated iridium(III) complexes involve lowest unoccupied molecular orbitals (LUMOs) localized on the neutral heterocycle of the C^N ligands, with the highest occupied molecular orbital (HOMO) more delocalized and consisting of a mixture of C^N aryl and iridium-centered  $d\pi$  orbitals with some degree of ancillary ligand character. 43 Consistent with this notion, for complexes with the same C^N ligand (pphen or piqCN), the observed  $E_{red}$  values occur at very similar potentials and are likewise nearly identical to the values we previously recorded for other complexes with the same C^N ligands. 39 The first reduction occurs between -2.07 and -2.17 V when C^N = pphen and between -1.65 and -1.69 V when C^N = piqCN. For the complex pphen-8OQ and all three piqCN complexes, there are two one-electron reduction waves and both are reversible, consistent with one electron being added to each C^N ligand's  $\pi^*$  orbital. In the remaining three pphen complexes, only the first reduction was clearly resolved due to the limited cathodic solvent window of dichloromethane.

The one-electron, formal  $Ir^{IV}/Ir^{III}$  oxidation potential,  $E_{ox}$  is mildly responsive to the anionic donor on the quinoline-based ancillary ligand. The  $E_{ox}$  value is most positive in the complexes where L^X = 8COOQ, with  $E_{ox}$  = +0.55 V (C^N = pphen) and +  $0.71 \text{ V (C}^{\text{N}} = \text{piqCN})$ , signifying that the carboxylate donor in this ancillary ligand is less electron-rich than the others and does not destabilize the HOMO to as great of an extent. This leads to the 8COOQ complexes having the largest electrochemical HOMO-LUMO gaps ( $\Delta E_{\rm H-L}$ ) in the series. The remaining complexes with aryloxy or amidate donors have  $E_{\rm ox}$  values that span a relatively narrow range of +0.26 to 0.42 V and, similarly,  $\Delta E_{\mathrm{H-L}}$  gaps that are within 110 mV of each other for a given C^N ligand. At parity of the ancillary ligand, the  $E_{ox}$  values are 110-160 mV more positive when C^N = piqCN, indicating some effect of the electron-withdrawing cyano substituent on the HOMO energy. Compared to previous pphen and piqCN complexes we have described where the electron-rich ancillary ligands are  $\beta$ -ketoiminate,  $\beta$ -diketiminate, and oramidinate derivatives,<sup>39</sup> most complexes described here have slightly more positive  $E_{ox}$  values and slightly larger electrochemical HOMO-LUMO gaps.

**DFT Calculations.** DFT calculations were performed on the representative compound **piqCN-8OQ** to investigate the composition of the frontier orbitals. The highest occupied Kohn–Sham orbital (HOMO) and the lowest unoccupied Kohn–Sham orbital (LUMO) are depicted in Figure 2, and Figure S2 shows a detailed Kohn–Sham frontier orbital diagram. The DFT calculations reveal that the LUMO is almost entirely centered on one C^N ligand, and the LUMO+1 is nearly degenerate and localized on the second C^N ligand. These observations are consistent with CV results described above that

#### piqCN-8OQ

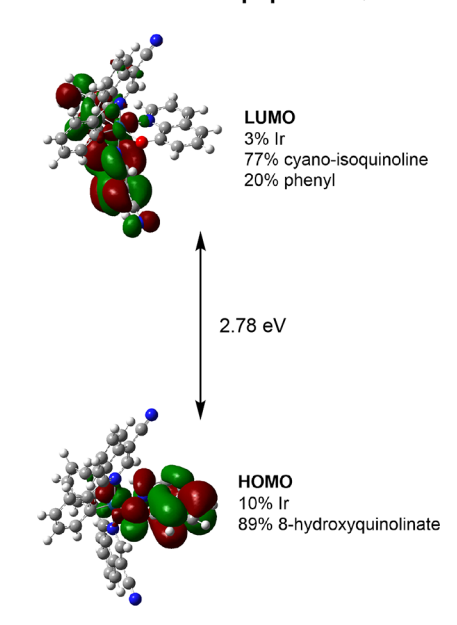


**Figure 2.** Kohn—Sham frontier orbitals of **piqCN-8OQ** at contour level of 0.02 au. Orbital compositions and computed HOMO—LUMO energy gaps are shown, with percentages representing electron density. The hybrid PBE0 exchange-correlation functional, TZVP (nonmetal atoms) and SDD (Ir) basis sets, and IEFPCM solvation (toluene) were used in the computation.

show one or two closely spaced reduction waves, indicating minimally altered LUMO energies across the series with the same C^N ligand. In contrast, the HOMO involves majority density from the 8-hydroxyquinoline ancillary ligand (89%), with only 10% arising from Ir 5d orbitals. This is likewise in line with the experimental electrochemical properties, as variations in the ancillary ligand significantly influence the one-electron oxidation potential and associated HOMO energy. The HOMO in piqCN-8OQ is more ligand-localized than was previously calculated in structurally related compounds. In  $Ir(piq)_2(L^X)$ compounds with electron-rich amidiante,  $\beta$ -ketoiminate, and  $\beta$ diketiminate ancillary ligands, the HOMO was extensively delocalized over the L^X ligand, the Ir center, and the C^N ligands, and even in the extreme case of  $\beta$ -diketiminate, the HOMO was 80% L^X and 17% Ir, more delocalized than that of piqCN-8OQ.

**Photophysical Properties.** The UV-vis absorption spectra of all complexes were recorded in room-temperature toluene solutions and are presented in Figure 3 below. In the absorption spectra of all complexes, strong bands in the ultraviolet region, below 400 nm, are assigned to  $\pi \to \pi^*$  transitions of the conjugated ligands. A collection of overlapping absorption features extending further into the visible region, beyond 500 nm, are attributed to spin-allowed and spin-forbidden charge-transfer transitions. The low-energy bands seem to correlate with electrochemical HOMO-LUMO gaps (see above), occurring at longer wavelengths when C^N = piqCN.

Photoluminescence spectra of the seven iridium(III) complexes were recorded in toluene at room temperature with 420 nm excitation, as shown in Figure 4, with the data summarized in Table 2. Excitation spectra were also recorded and are displayed in Figures S3—S9. In every case, there is good overlay between the absorption and emission spectra, indicating

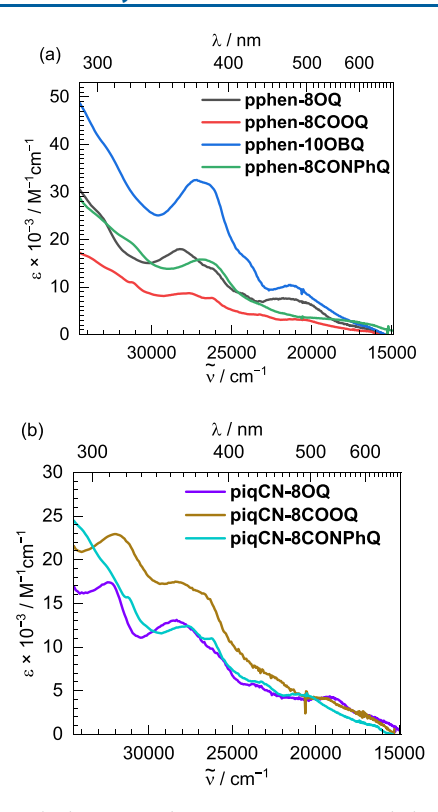


**Figure 3.** Overlaid UV—vis absorption spectra recorded in toluene at room temperature. Spectra are organized by cyclometalating ligands, with (a) showing the complexes with  $C^N = pphen$ , and (b) showing those with  $C^N = piqCN$ .

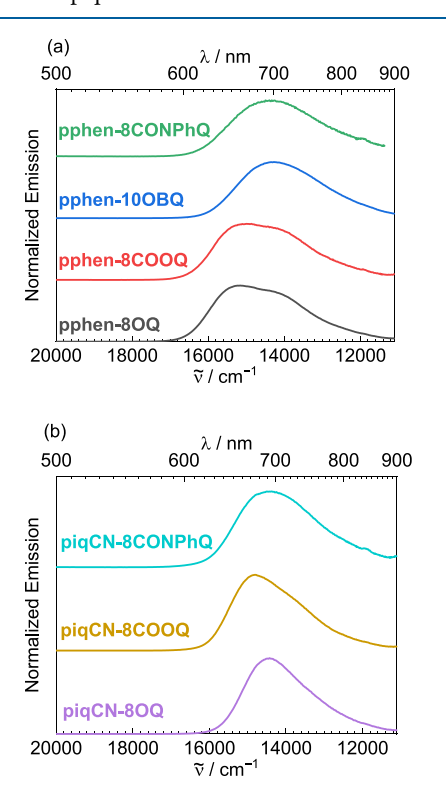


**Figure 4.** Stacked room-temperature photoluminescence spectra of complexes with (a) C^N = pphen and (b) C^N = piq, recorded in toluene. Samples were excited at  $\lambda_{ex}$  = 420 nm.

that impurities are not contributing to the observed luminescence and that Kasha's rule is followed. In previous

Table 2. Room-Temperature Photoluminescence Data Recorded in Toluene

complex	$\lambda_{\rm em}$ (nm)	$\Phi_{ ext{PL}}$	τ (μs)	$(k_{\rm r} \times 10^{-5}/{\rm s}^{-1})/(k_{\rm nr} \times 10^{-5}/{\rm s}^{-1})$
pphen-8OQ	660, 700(sh)	0.28	1.4	1.4/5.1
pphen-8COOQ	667, 696(sh)	0.19	1.1	1.7/7.4
pphen-10OBQ	701	0.29	0.97	3.0/7.3
pphen- 8CONPhQ	697	0.018	0.70	0.26/14
piqCN-8OQ	693	0.42	0.55	7.6/10.5
piqCN- 8COOQ	676	0.27	0.78	3.5/9.4
piqCN- 8CONPhQ	696	0.047	0.80	0.59/12

work with these same quinoline-derived ancillary ligands paired with the cyclometalating ligand 2-(10-phenanthridine)-benzothiophene (btph), we observed good quantum yields in the NIR region (PL max  $\lambda > 700$  nm), with Ir(btph)<sub>2</sub>(8OQ) having the highest photoluminescence quantum yield in that series, 0.36 in THF. However, as seen in the previous studies, the complexes with C^N ligands involving a thiophene-containing cyclometalated aryl ring, including btph, have excited states that are more C^N ligand-localized with less charge-transfer character, resulting in excited state dynamics that vary little with the ancillary ligand structure in most cases. Hotophysical properties of complexes supported by the quinoline-derived ancillary ligands while employing C^N ligands that can result in DR-NIR phosphorescence but should be more responsive to the ancillary ligand structure.

The emission peak of most pphen and piqCN complexes reported here occurs in the deep-red region (660–697 nm), the exception being pphen-10OBQ, where the peak occurs at 701 nm and can be reasonably assigned as NIR emission. Peak shapes are broad and featureless in general, although a poorly resolved vibronic structure is evident in pphen-80Q, pphen-**8COOQ**, and piqCN-8COOQ. The  $\Phi_{PL}$  values are variable and for most are similar to or lower than those of previously reported complexes with  $C^N = btph.^{42}$  A noteworthy exception is piqCN-8OQ, for which  $\Phi_{PL}$  = 0.42 with a peak wavelength of 693 nm, a higher quantum yield than we previously achieved with the btph cyclometalating ligand. To further interpret the variable  $\Phi_{PL}$  values and further contextualize the excited-state dynamics, PL lifetimes were recorded (Figures S10-S16). The resulting  $k_r$  and  $k_{nr}$  values, summarized in Table 1, are compared to those of the previously reported complex Ir(btph)<sub>2</sub>(8OQ), for which  $k_r = 1.8 \times 10^5 \text{ s}^{-1}$  and  $k_{nr} = 3.2 \times 10^5 \text{ s}^{-1}$ . The  $k_r$  values in the pphen and piqCN complexes are quite responsive to the ancillary ligand structure, and most have similar or higher values than the reference complex, with the complex piqCN-8OQ showing the biggest increase to  $7.6 \times 10^5$  s<sup>-1</sup>. One noticeable trend in  $k_r$  values is that those with the amidate-substituted ancillary ligand 8CONPhQ are significantly smaller than the rest,  $<10^5$  s<sup>-1</sup>. However, regardless of their  $k_r$  values, all the complexes have much higher  $k_{\rm nr}$  values than the reference complex, ranging from 5.1 to  $14 \times 10^5$  s<sup>-1</sup>, which is responsible for the attenuation in quantum yield seen in most cases. That said, a key takeaway is that whereas the btph complexes in our previous study showed minimal dependence of the radiative and nonradiative decay rates on the ancillary ligand structure, those with pphen and piqCN exhibit a wider range of  $k_r$  and  $k_{nr}$  values.

The photoluminescence lifetimes ( $\tau$ ) of the new complexes described here, likewise collected at room temperature, span 0.55–1.4  $\mu$ s. In most cases, these values are significantly shorter than those of the previously described  $Ir(C^N)_2(L^X)$  complexes with  $C^N = btph$  partnered with quinoline-derived ancillary ligands and slightly longer than those of analogues where pphen and piqCN are paired up with other classes of electron-rich ancillary ligands.

To better understand the excited states, the Franck-Condon singlet and triplet excited states of piqCN-8OQ were computed via time-dependent DFT. The calculations demonstrate that the lowest-energy singlet excited state consists of a clean LUMO ← HOMO one-electron transition at 595 nm. The first Franck-Condon triplet, calculated at 621 nm, consists of two singleparticle transitions mixed through configuration interaction, as shown in Figure S17. Natural transition orbitals indicate a mixed metal-ligand-to-ligand charge transfer (MLL'CT) origin of this triplet state, which is intermediate between pure MLCT and pure LL'CT. Charge transfers from iridium, one cyclometalating ligand, and 8-hydroxyquiniline to the same cyclometalating ligand. Calculation of the spin density of the first (FC) triplet indicates that spin delocalizes over the complex, with 33% of spin density on iridium, 19% across the cyclometalating ligands, and nearly 20% on 8-hydroxyquinoline. A spin density plot appears as Figure S18, Supporting Information.

#### CONCLUSIONS

Here, seven new bis-cyclometalated iridium deep-red phosphorescent emitters are reported, all supported by substituted quinoline ancillary ligands. The excited-state properties of the compounds were characterized. Our goal was to synthesize complexes with emission in the deep-red to NIR region with good quantum yields and fast radiative rates as promising candidates for applications that require phosphorescence in these regions. Most of the complexes exhibit luminescence in the deep-red region with maxima between 660 and 701 nm, and except for the two complexes with the amide-substituted 8CONPhQ ancillary ligand, the quantum yields are higher than 0.19 and reasonably good for this region of the spectrum. The excited-state kinetics and photoluminescence quantum yields depend strongly on the ancillary ligands, and the highest quantum yield was obtained from the complex Ir- $(piqCN)_2(8OQ)$  (piqCN-80Q), with  $\Phi_{PL} = 0.42$ . This work shows that quinoline-based chelating ligands substituted with variable anionic donors can influence the excited-state dynamics of cyclometalated iridium complexes when paired with appropriate cyclometalating ligands, promoting efficient luminescence in the deep-red region of the spectrum.

## EXPERIMENTAL SECTION

**Materials.** All reactions were executed in a nitrogen-filled glovebox operating at <1 ppm of  $O_2$  and  $H_2O$  or on dual vacuum/nitrogen manifold using standard Schlenk techniques. All starting materials and reagents were obtained from commercial sources and used without further purification. Solvents for reactions and optical measurements were deoxygenated and dried by the method of Grubbs, sparging with argon and passing through dual alumina columns on a commercial solvent purification system (SPS). Purified solvents were stored in the glovebox over 3 Å molecular sieves. The cyclometalating ligand, 1-phenylisoquinoline-4-carbonitrile (piqCN), was synthesized according to literature procedures. Cyclometalated iridium dimers [Ir- $(C^N)_2(\mu-Cl)_2$  ( $C^N = 6$ -phenylphenanthridine (pphen) and piqCN) were prepared by the method of Nonoyama, feluxing IrCl<sub>3</sub>·nH<sub>2</sub>O with 2–2.5 equiv of the cyclometalating ligand in a 3:1

mixture of 2-ethoxyethanol and water. The potassium salt of the 8OQ ligand, 8OQK, was prepared by the general procedure as described previously by our lab.  $^{42}$  Tetrabutylammonium hexafluorophosphate (TBAPF $_6$ ) was recrystallized from hot ethanol, and ferrocene was sublimed at ambient pressure before use in electrochemical experiments.

Physical Methods. <sup>1</sup>H NMR spectra (shown in Figures S19–S25) were recorded at room temperature using a JEOL ECA-400 or ECA-500 NMR spectrometer. UV-vis absorption spectra were recorded in toluene solutions in screw-capped quartz cuvettes using an Agilent Carey 8454 UV-vis spectrophotometer. To determine the molar absorptivity values, absorption spectra were recorded on samples of varying concentration, and the data at a peak wavelength was fit via the Beer-Lambert Law. Since most of the compounds were isolated as solvates (see NMR spectra in Figures S19-S25), NMR integration was used to estimate the solvent content, and the molar masses were adjusted accordingly when calculating sample concentrations for molar absorptivity determination. Luminescence lifetimes were measured with a Horiba DeltaFlex Lifetime System using 455 nm pulsed diode excitation. Steady-state emission spectra were recorded using a Horiba FluoroMax-4 spectrofluorometer with appropriate long-pass filters to exclude stray excitation light from detection. In order to exclude air, samples for emission spectra were prepared in a nitrogen-filled glovebox using anhydrous solvents that had been previously deoxygenated and dried in the SPS. Samples for room-temperature emission were housed in 1 cm quartz cuvettes with septum-sealed screw caps, and samples for low-temperature emission were contained in a custom quartz EPR tube with a high-vacuum valve and immersed in liquid nitrogen using a finger Dewar. Solution quantum yields were determined relative to a standard of tetraphenylporphyrin in toluene, which has a reported fluorescence quantum yield  $(\Phi_{\rm F})$  of 0.11. <sup>46</sup> Cyclic voltammetry (CV) measurements were performed with a CH Instruments 602E potentiostat interfaced with a nitrogen glovebox via wire feedthroughs. Samples were dissolved in THF or CH<sub>2</sub>Cl<sub>2</sub> with 0.1 M TBAPF<sub>6</sub> as a supporting electrolyte. A 3 mm diameter glassy carbon working electrode, a platinum wire counter electrode, and a silver wire pseudo-reference electrode were used. Potentials were referenced to an internal standard of ferrocene.

**DFT Calculations.** Static density-functional theory (DFT) calculations were carried out on the complex **piqCN-8OQ**. The singlet ground-state optimization was spin-restricted, and harmonic frequency calculations verified that the singlet ground state was an energy minimum. The calculations employed the hybrid exchange-correlation functional of Perdew, Burke, and Ernzerhof (PBE0).<sup>47</sup> The TZVP basis set was used for all nonmetal atoms, <sup>48,49</sup> and the SDD basis set and effective core potential were used for iridium.<sup>50</sup> Continuum solvation was imposed using the integral equation formalism of the polarizable continuum model.<sup>51–54</sup> Standard Mulliken<sup>55</sup> and NPA<sup>56</sup> population analyses<sup>57,58</sup> were performed with the AOMix-CDA program of Gorelsky.<sup>59,60</sup> All computations were performed within Gaussian16 rev. A.2.<sup>61</sup>

Synthesis of pphen-80Q. A mixture of 2 mL of dichloromethane, 2 mL of ethanol, and 1 mL of triethylamine was deoxygenated for 30 min by bubbling with nitrogen.  $[Ir(pphen)_2(\mu-Cl)]_2$  (50 mg, 0.034 mmol) and 8-hydroxyquinoline (0.12 mmol, 3.5 equiv) were added. The reaction mixture was heated to reflux with a bath temperature of 80 °C and stirred overnight. After cooling to room temperature, the reaction solution was concentrated to dryness in vacuo. Four milliliters of methanol was added, and the mixture was stored in the refrigerator overnight. The solids were collected by filtration and washed with methanol, hexane, and pentane. Yield: 21 mg (36%). <sup>1</sup>H NMR (500 MHz, CDCl<sub>3</sub>)  $\delta$ : 9.23 (d, J = 8.0 Hz, 1H, ArH), 9.09 (d, J = 8.0 Hz, 2H, ArH), 8.54 (t, J = 7.6 Hz, 2H, ArH), 8.37 (d, J = 8.5 Hz, 1H, ArH), 8.30 (d, J = 8.0 Hz, 2H, ArH), 8.25 (d, J = 8.0 Hz, 1H, ArH), 8.20 - 8.23 (m, J = 8.0 Hz, 2H, ArH)1H, ArH), 7.91 (d, J = 9.0 Hz, 1H, ArH), 7.75 - 7.89 (m, 5H, ArH), 7.63(d, J = 8.5 Hz, 1H, ArH), 6.98-7.05 (m, 3H, ArH), 6.94 (t, J = 8.0 Hz,1H, ArH), 6.87 (t, J = 8.0 Hz, 1H, ArH), 6.75 (t, J = 7.3 Hz, 1H, ArH), 6.64 (t, J = 7.5 Hz, 1H, ArH), 6.54 (d, J = 7.5 Hz, 1H, ArH), 6.43-6.49 $(m, 1H, ArH), 6.27-6.33 (m, 1H, ArH). HRMS-ESI (m/z): [M + Na]^+$ calcd for C<sub>47</sub>H<sub>30</sub>IrN<sub>3</sub>O, 868.1910; found, 868.1888.

Synthesis of pphen-8COOQ. A mixture of 2 mL of dichloromethane, 2 mL of ethanol, and 1 mL of triethylamine was deoxygenated for 30 min by bubbling with nitrogen.  $[Ir(pphen)_2(\mu-Cl)]_2$  (50 mg, 0.034 mmol) and 8-quinolinecarboxylic acid (0.12 mmol, 3.5 equiv) were added. The reaction mixture was heated to reflux with a bath temperature of 85 °C and stirred overnight. After cooling to room temperature, the solution was concentrated to dryness. Four milliliters of methanol was added, and the mixture was stored in the refrigerator overnight. The solids were filtered and washed with methanol, hexane, and pentane to yield the desired product. Yield: 12 mg (21%). <sup>1</sup>H NMR  $(400 \text{ MHz}, \text{CDCl}_3) \delta$ : 9.44 (d, J = 8.4 Hz, 1H, ArH), 9.19 (d, J = 8.4 Hz, 1H, ArH), 9.07 (d, J = 8.0 Hz, 1H, ArH), 8.72 - 8.76 (m, 1H, ArH), 8.65(d, J = 8.0 Hz, 1H, ArH), 8.58 (d, J = 8.8 Hz, 1H, ArH), 8.41 (d, J = 8.4)Hz, 1H, ArH), 8.20-8.32 (m, 3H, ArH), 8.16 (d, J = 7.6 Hz, 1H, ArH), 7.87-7.98 (m, 3H, ArH), 7.82 (t, J = 7.6 Hz, 2H, ArH), 7.41-7.65 (m, 3H, ArH), 6.93-7.18 (m, 6H, ArH), 6.90 (d, J = 7.6 Hz, 1H, ArH), 6.66(t, J = 7.6 Hz, 1H, ArH), 6.59 (t, J = 7.6 Hz, 1H, ArH), 6.45-6.52 (m,2H, ArH). HRMS-ESI (m/z):  $[M + Na]^+$  calcd for  $C_{48}H_{30}IrN_3O_{24}$ 896.1860; found, 896.1846.

Synthesis of pphen-100BQ. A mixture of 2 mL of dichloromethane, 2 mL of ethanol, and 1 mL of triethylamine were deoxygenated for 30 min by bubbling with nitrogen. [Ir(pphen)<sub>2</sub>(µ-Cl)  $_{2}$  (28 mg, 0.019 mmol) and 10-hydroxybenzo [h] quinoline (0.048 mmol, 2.5 equiv) were added. The reaction mixture was heated under reflux at 80 °C overnight. The reaction was cooled to room temperature, and the solution was concentrated to dryness. Four milliliters of methanol was added, and the mixture was stored in the refrigerator overnight. The solids were filtered and washed with methanol, hexane, and pentane to yield the desired product. Yield: 11 mg (33%). <sup>1</sup>H NMR (500 MHz, DMSO- $d_6$ )  $\delta$ : 9.83 (d, J = 9.0 Hz, 1H, ArH), 9.15 (d, J = 8.0 Hz, 1H, ArH), 8.94–9.05 (m, 2H, ArH), 8.73 (d, J= 8.5 Hz, 1H, ArH), 8.51 - 8.59 (m, 1H, ArH), 8.37 (d, J = 8.5 Hz, 1H,ArH), 8.25 (d, J = 8.0 Hz, 1H, ArH), 8.06–8.18 (m, 4H, ArH), 8.02 (t, J= 7.5 Hz, 1H, ArH), 7.87 - 7.93 (m, 2H, ArH), 7.51 (q, J = 8.0 Hz, 1H,ArH), 7.30 (t, J = 7.3 Hz, 1H, ArH), 7.11–7.19 (m, 3H, ArH), 6.99– 7.09 (m, 2H, ArH), 6.91-6.97 (m, 1H, ArH), 6.87 (d, J = 7.5 Hz, 1H,ArH), 6.75 (d, J = 8.5 Hz, 1H, ArH), 6.56 (q, 2H, ArH), 6.40 (t, J = 7.5Hz, 1H, ArH), 6.26-6.32 (m, 3H, ArH), 5.82-5.87 (m, 1H, ArH). HRMS-ESI (m/z):  $[M + Na]^+$  calcd for  $C_{51}H_{32}IrN_3O$ , 918.2067; found, 918.2045.

**Synthesis of pphen-8CONPhQ.** In the glovebox,  $[Ir(pphen)_2(\mu-Cl)]_2$  (22 mg, 0.015 mmol) and *N*-phenyl-8-quinolinecarboxamide (0.045 mmol, 3.0 equiv) were suspended in 5 mL of dichloromethane with excess NaOCH<sub>3</sub>. After stirring overnight at room temperature, the resulting dark solution was filtered and concentrated in vacuo. The final product was separated by column chromatography, using alumina as the stationary phase and  $CH_2Cl_2$ /ethyl acetate (1:1) as the eluent. Yield: 6.9 mg (24%). <sup>1</sup>H NMR (400 MHz, CDCl<sub>3</sub>)  $\delta$ : 9.55 (d, J = 8.0 Hz, 1H, ArH), 9.45 (d, J = 8.8 Hz, 1H, ArH), 8.70 (q, J = 8.8 Hz, 2H, ArH), 8.52 (d, J = 7.2 Hz, 1H, ArH), 8.25 (d, J = 8.0 Hz, 1H, ArH), 8.12–8.22 (m, 1H, ArH), 7.14–7.21 (m, 2H, ArH), 6.93–7.00 (m, 2H, ArH), 6.78–6.90 (m, 2H, ArH), 6.65–6.76 (m, 2H, ArH), 6.54–6.60 (m, 1H, ArH), 6.30–6.44 (m, 5H, ArH), 6.19–6.24 (m, 1H, ArH). HRMS-ESI (m/z):  $[M+H]^+$  calcd for  $C_{54}H_{35}IrN_4O$ , 948.2513; found, 949.2509.

**Synthesis of piqCN-80Q.** In the glovebox,  $[Ir(piqCN)_2(\mu-Cl)]_2$  (27 mg, 0.018 mmol) was suspended in 4 mL of THF. A solution of 8OQK (19 mg, 0.066 mmol, 3.7 equiv) in 4 mL THF was added slowly to the stirred mixture. After stirring overnight at room temperature, the resulting brown solution was concentrated in vacuo. The dark residue was extracted with 6 mL of toluene and filtered through Celite. The toluene was removed under vacuum, and the solid was retrieved. Further purification was done by dissolving in THF and slowly adding pentane to precipitate out the side product. The final product was retrieved upon concentration. Yield: 12 mg (35%). <sup>1</sup>H NMR (500 MHz,  $C_6D_6$ ) δ: 9.49 (s, 1H, ArH), 8.38 (d, 1H, ArH), 8.27–8.34 (m, 1H, ArH), 7.98 (t, J = 8.3 Hz, 2H, ArH), 7.83 (s, 1H, ArH), 7.58–7.64 (m, 2H, ArH), 7.48–7.53 (m, 1H, ArH), 7.17–7.27 (m, 3H, ArH), 6.79–6.95 (m, 8H, ArH), 6.74 (t, J = 7.0 Hz, 1H, ArH), 6.65 (t, J = 7.5 Hz, 1H, ArH), 6.57 (d, J = 8.0 Hz, 1H, ArH), 6.46–6.52 (m, 1H, ArH),

6.16–6.21 (m, 1H, ArH). HRMS-ESI (m/z):  $[M + Na]^+$  calcd for  $C_{41}H_{24}IrN_5O$ , 818.1502; found, 818.1484.

Synthesis of piqCN-8COOQ. A mixture of 2 mL of dichloromethane, 2 mL of ethanol, and 1 mL of triethylamine was deoxygenated for 30 min by bubbling with nitrogen.  $[Ir(piqCN)_2(\mu-Cl)]_2$  (26 mg, 0.019 mmol) and 8-quinolinecarboxylic acid (0.067 mmol, 3.5 equiv) were added. The reaction mixture was bought to reflux with a bath temperature of 80 °C and heated overnight. The reaction was cooled to room temperature, and the solution was concentrated to dryness. Four milliliters of methanol was added, and the mixture was stored in the refrigerator overnight. The solids were filtered and washed with methanol, hexane, and pentane to yield the desired product. Yield: 16 mg (50%). <sup>1</sup>H NMR (500 MHz, CDCl<sub>3</sub>)  $\delta$ : 9.46 (s, 1H, ArH), 9.05 (d, J = 8.5 Hz, 1H, ArH), 8.98 (t, J = 7.0 Hz, 2H, ArH), 8.36 (d, J = 8.0 Hz,1H, ArH), 8.32 (d, J = 8.5 Hz, 2H, ArH), 8.14 (d, J = 8.0 Hz, 2H, ArH), 7.83-8.03 (m, 6H, ArH), 7.76 (t, J = 8.0 Hz, 1H, ArH), 7.60 (s, 1H, ArH), 7.06–7.14 (m, 2H, ArH), 6.97 (t, J = 7.5 Hz, 1H, ArH), 6.81 (t, J= 7.5 Hz, 1H, ArH), 6.73 (t, J = 7.5 Hz, 1H, ArH), 6.47 (d, J = 8.0 Hz,1H, ArH), 6.13 (d, J = 8.0 Hz, 1H, ArH). HRMS-ESI (m/z):  $[M + Na]^{+}$ calcd for C<sub>42</sub>H<sub>24</sub>IrN<sub>5</sub>O<sub>2</sub>, 846.1451; found, 846.1437.

**Synthesis of piqCN-8CONPhQ.** In the glovebox,  $[Ir(piqCN)_2(\mu-$ Cl)<sub>2</sub> (20 mg, 0.015 mmol) and N-phenyl-8-quinolinecarboxamide (0.045 mmol, 3.0 equiv) were suspended in 5 mL of THF with excess NaH. After stirring for 3 h at 80 °C, the resulting dark solution was filtered through Celite and concentrated in vacuo. The product was redissolved in a minimum amount of dichloromethane, and pentane was slowly added in to precipitate out the final product. Yield: 11 mg (42%). <sup>1</sup>H NMR (400 MHz, CDCl<sub>3</sub>)  $\delta$ : 9.60 (s, 1H, ArH), 9.13 (s, 1H, ArH), 9.05–9.11 (m, 1H, ArH), 8.55–8.63 (m, 3H, ArH), 8.31 (d, *J* = 8.0 Hz, 1H, ArH), 8.09 (d, J = 8.4 Hz, 1H, ArH), 8.01–8.06 (m, 1H, ArH), 7.88–7.96 (m, 2H, ArH), 7.76–7.85 (m, 2H, ArH), 7.60–7.73 (m, 4H, ArH), 7.01-7.07 (m, 1H, ArH), 6.91-6.97 (m, 1H, ArH), 6.75-6.86 (m, 2H, ArH), 6.57-6.63 (m, 1H, ArH) 6.46 (t, J = 7.4 Hz, 1H, ArH), 6.32-6.43 (m, 3H, ArH), 6.17-6.22 (m, 1H, ArH), 6.01-6.11 (m, 2H, ArH). HRMS-ESI (m/z): [M + H]<sup>+</sup> calcd for C<sub>48</sub>H<sub>29</sub>IrN<sub>6</sub>O, 899.2105; found, 899.2101.

## ASSOCIATED CONTENT

## Supporting Information

The Supporting Information is available free of charge at https://pubs.acs.org/doi/10.1021/acs.inorgchem.3c00670.

Cyclic voltammograms, Kohn—Sham orbital diagram from DFT calculations, excitation spectra overlaid with UV—vis absorption spectra, time-resolved photoluminescence data, computed Franck—Condon triplet-state NTOs and spin density, and NMR spectra (PDF)

Output XYZ file from DFT geometry optimization (XYZ)

## AUTHOR INFORMATION

# **Corresponding Author**

Thomas S. Teets — Department of Chemistry, University of Houston, Houston, Texas 77204-5003, United States;
ocid.org/0000-0002-7471-8467; Email: tteets@uh.edu

# Authors

Sungwon Yoon — Department of Chemistry, University of Houston, Houston, Texas 77204-5003, United States

Thomas G. Gray — Department of Chemistry, Case Western Reserve University, Cleveland, Ohio 44106, United States;
orcid.org/0000-0003-1756-8877

Complete contact information is available at: https://pubs.acs.org/10.1021/acs.inorgchem.3c00670

#### **Author Contributions**

The manuscript was written through contributions of all authors. All authors have given approval to the final version of the manuscript.

#### **Notes**

The authors declare no competing financial interest.

## ACKNOWLEDGMENTS

The authors acknowledge the National Science Foundation (grant no. CHE-1846831) and the Welch Foundation (grant no. E-1887) for funding this work. T.G.G. acknowledges the Air Force Office of Scientific Research, contract FA9550-22-1-0436, for funding.

#### REFERENCES

- (1) Prier, C. K.; Rankic, D. A.; MacMillan, D. W. C. Visible Light Photoredox Catalysis with Transition Metal Complexes: Applications in Organic Synthesis. *Chem. Rev.* **2013**, *113*, 5322–5363.
- (2) Shon, J.-H.; Kim, D.; Rathnayake, M. D.; Sittel, S.; Weaver, J.; Teets, T. S. Photoredox Catalysis on Unactivated Substrates with Strongly Reducing Iridium Photosensitizers. *Chem. Sci.* **2021**, *12*, 4069–4078.
- (3) Bozic-Weber, B.; Constable, E. C.; Housecroft, C. E. Light Harvesting with Earth Abundant D-Block Metals: Development of Sensitizers in Dye-Sensitized Solar Cells (DSCs). *Coord. Chem. Rev.* **2013**, 257, 3089–3106.
- (4) Polo, A. S.; Itokazu, M. K.; Murakami Iha, N. Y. Metal Complex Sensitizers in Dye-Sensitized Solar Cells. *Coord. Chem. Rev.* **2004**, *248*, 1343–1361.
- (5) Mills, I. N.; Porras, J. A.; Bernhard, S. Judicious Design of Cationic, Cyclometalated Ir(III) Complexes for Photochemical Energy Conversion and Optoelectronics. *Acc. Chem. Res.* **2018**, *51*, 352–364.
- (6) Ma, D.-L.; Ma, V. P.-Y.; Chan, D. S.-H.; Leung, K.-H.; He, H.-Z.; Leung, C.-H. Recent Advances in Luminescent Heavy Metal Complexes for Sensing. *Coord. Chem. Rev.* **2012**, *256*, 3087–3113.
- (7) Liu, Z.; He, W.; Guo, Z. Metal Coordination in Photoluminescent Sensing. *Chem. Soc. Rev.* **2013**, 42, 1568–1600.
- (8) Iridium(III) in Optoelectronic and Photonics Applications; Zysman-Colman, E., Ed.; John Wiley & Sons, Inc: Chichester, West Sussex, 2017.
- (9) Zhang, Y.; Wang, Y.; Song, J.; Qu, J.; Li, B.; Zhu, W.; Wong, W.-Y. Near-Infrared Emitting Materials via Harvesting Triplet Excitons: Molecular Design, Properties, and Application in Organic Light Emitting Diodes. *Adv. Opt. Mater.* **2018**, *6*, 1800466.
- (10) You, C.; Liu, D.; Zhu, M.; Yu, J.; Zhang, B.; Liu, Y.; Wang, Y.; Zhu, W.  $\sigma$ – $\pi$  and p– $\pi$  Conjugation Induced NIR-Emitting Iridium-(III) Complexes Anchored by Flexible Side Chains in a Rigid Dibenzo[a,c]Phenazine Moiety and Their Application in Highly Efficient Solution-Processable NIR-Emitting Devices. *J. Mater. Chem.* C 2020, 8, 7079–7088.
- (11) Lee, L. C.-C.; Lo, K. K.-W. Luminescent and Photofunctional Transition Metal Complexes: From Molecular Design to Diagnostic and Therapeutic Applications. *J. Am. Chem. Soc.* **2022**, *144*, 14420–14440.
- (12) Heinemann, F.; Karges, J.; Gasser, G. Critical Overview of the Use of Ru(II) Polypyridyl Complexes as Photosensitizers in One-Photon and Two-Photon Photodynamic Therapy. *Acc. Chem. Res.* **2017**, *50*, 2727–2736.
- (13) Tung, Y.-L.; Lee, S.-W.; Chi, Y.; Chen, L.-S.; Shu, C.-F.; Wu, F.-I.; Carty, A. J.; Chou, P.-T.; Peng, S.-M.; Lee, G.-H. Organic Light-Emitting Diodes Based on Charge-Neutral RuII Phosphorescent Emitters. *Adv. Mater.* **2005**, *17*, 1059–1064.
- (14) Wang, Y.; Liu, S.; Pinto, M. R.; Dattelbaum, D. M.; Schoonover, J. R.; Schanze, K. S. Excited-State Structure and Delocalization in Ruthenium(II)—Bipyridine Complexes That Contain Phenyleneethynylene Substituents. *J. Phys. Chem. A* **2001**, *105*, 11118—11127.

- (15) Yuan, Y.; Liao, J.-L.; Ni, S.-F.; Jen, A. K.-Y.; Lee, C.-S.; Chi, Y. Boosting Efficiency of Near-Infrared Organic Light-Emitting Diodes with Os(II)-Based Pyrazinyl Azolate Emitters. *Adv. Funct. Mater.* **2020**, 30, 1906738.
- (16) Liao, J.-L.; Chi, Y.; Yeh, C.-C.; Kao, H.-C.; Chang, C.-H.; Fox, M. A.; Low, P. J.; Lee, G.-H. Near Infrared-Emitting Tris-Bidentate Os(II) Phosphors: Control of Excited State Characteristics and Fabrication of OLEDs. *J. Mater. Chem. C* **2015**, *3*, 4910–4920.
- (17) Lee, T.-C.; Hung, J.-Y.; Chi, Y.; Cheng, Y.-M.; Lee, G.-H.; Chou, P.-T.; Chen, C.-C.; Chang, C.-H.; Wu, C.-C. Rational Design of Charge-Neutral, Near-Infrared-Emitting Osmium(II) Complexes and OLED Fabrication. *Adv. Funct. Mater.* **2009**, *19*, 2639–2647.
- (18) Roy, S.; Lopez, A. A.; Yarnell, J. E.; Castellano, F. N. Metal—Metal-to-Ligand Charge Transfer in Pt(II) Dimers Bridged by Pyridyl and Quinoline Thiols. *Inorg. Chem.* **2022**, *61*, 121–130.
- (19) Wang, S. F.; Yuan, Y.; Wei, Y.-C.; Chan, W.-H.; Fu, L.-W.; Su, B.-K.; Chen, I.-Y.; Chou, K.-J.; Chen, P.-T.; Hsu, H.-F.; Ko, C.-L.; Hung, W.-Y.; Lee, C.-S.; Chou, P.-T.; Chi, Y. Highly Efficient Near-Infrared Electroluminescence up to 800 Nm Using Platinum(II) Phosphors. *Adv. Funct. Mater.* **2020**, *30*, 2002173.
- (20) Wang, S. F.; Fu, L.-W.; Wei, Y.-C.; Liu, S.-H.; Lin, J.-A.; Lee, G.-H.; Chou, P.-T.; Huang, J.-Z.; Wu, C.-I.; Yuan, Y.; Lee, C.-S.; Chi, Y. Near-Infrared Emission Induced by Shortened Pt—Pt Contact: Diplatinum(II) Complexes with Pyridyl Pyrimidinato Cyclometalates. *Inorg. Chem.* **2019**, *58*, 13892—13901.
- (21) Tuong Ly, K.; Chen-Cheng, R.-W.; Lin, H.-W.; Shiau, Y.-J.; Liu, S.-H.; Chou, P.-T.; Tsao, C.-S.; Huang, Y.-C.; Chi, Y. Near-Infrared Organic Light-Emitting Diodes with Very High External Quantum Efficiency and Radiance. *Nat. Photonics* **2017**, *11*, 63–68.
- (22) Graham, K. R.; Yang, Y.; Sommer, J. R.; Shelton, A. H.; Schanze, K. S.; Xue, J.; Reynolds, J. R. Extended Conjugation Platinum(II) Porphyrins for Use in Near-Infrared Emitting Organic Light Emitting Diodes. *Chem. Mater.* **2011**, 23, 5305–5312.
- (23) Rossi, E.; Murphy, L.; Brothwood, P. L.; Colombo, A.; Dragonetti, C.; Roberto, D.; Ugo, R.; Cocchi, M.; Williams, J. A. G. Cyclometallated Platinum(II) Complexes of 1,3-Di(2-Pyridyl)-Benzenes: Tuning Excimer Emission from Red to near-Infrared for NIR-OLEDs. J. Mater. Chem. 2011, 21, 15501–15510.
- (24) Kitzmann, W. R.; Ramanan, C.; Naumann, R.; Heinze, K. Molecular Ruby: Exploring the Excited State Landscape. *Dalton Trans.* **2022**, *51*, 6519–6525.
- (25) Reichenauer, F.; Wang, C.; Förster, C.; Boden, P.; Ugur, N.; Báez-Cruz, R.; Kalmbach, J.; Carrella, L. M.; Rentschler, E.; Ramanan, C.; Niedner-Schatteburg, G.; Gerhards, M.; Seitz, M.; Resch-Genger, U.; Heinze, K. Strongly Red-Emissive Molecular Ruby [Cr(bpmp)<sub>2</sub>]<sup>3+</sup> Surpasses [Ru(bpy)<sub>3</sub>]<sup>2+</sup>. *J. Am. Chem. Soc.* **2021**, *143*, 11843–11855.
- (26) Otto, S.; Grabolle, M.; Förster, C.; Kreitner, C.; Resch-Genger, U.; Heinze, K. [Cr(ddpd)<sub>2</sub>]<sup>3+</sup>: A Molecular, Water-Soluble, Highly NIR-Emissive Ruby Analogue. *Angew. Chem., Int. Ed.* **2015**, *54*, 11572–11576
- (27) Ho, C.-L.; Li, H.; Wong, W.-Y. Red to Near-Infrared Organometallic Phosphorescent Dyes for OLED Applications. *J. Organomet. Chem.* **2014**, *751*, 261–285.
- (28) Tsuboyama, A.; Iwawaki, H.; Furugori, M.; Mukaide, T.; Kamatani, J.; Igawa, S.; Moriyama, T.; Miura, S.; Takiguchi, T.; Okada, S.; Hoshino, M.; Ueno, K. Homoleptic Cyclometalated Iridium Complexes with Highly Efficient Red Phosphorescence and Application to Organic Light-Emitting Diode. *J. Am. Chem. Soc.* **2003**, *125*, 12971–12979.
- (29) Fan, C.-H.; Sun, P.; Su, T.-H.; Cheng, C.-H. Host and Dopant Materials for Idealized Deep-Red Organic Electrophosphorescence Devices. *Adv. Mater.* **2011**, *23*, 2981–2985.
- (30) Lamansky, S.; Djurovich, P.; Murphy, D.; Abdel-Razzaq, F.; Lee, H.-E.; Adachi, C.; Burrows, P. E.; Forrest, S. R.; Thompson, M. E. Highly Phosphorescent Bis-Cyclometalated Iridium Complexes: Synthesis, Photophysical Characterization, and Use in Organic Light Emitting Diodes. J. Am. Chem. Soc. 2001, 123, 4304–4312.
- (31) Yoshihara, T.; Murayama, S.; Masuda, T.; Kikuchi, T.; Yoshida, K.; Hosaka, M.; Tobita, S. Mitochondria-Targeted Oxygen Probes

- Based on Cationic Iridium Complexes with a 5-Amino-1, 10-Phenanthroline Ligand. *J. Photochem. Photobiol. Chem.* **2015**, 299, 172–182.
- (32) Chen, Z.; Zhang, H.; Wen, D.; Wu, W.; Zeng, Q.; Chen, S.; Wong, W.-Y. A Simple and Efficient Approach toward Deep-Red to near-Infrared-Emitting Iridium(III) Complexes for Organic Light-Emitting Diodes with External Quantum Efficiencies of over 10%. *Chem. Sci.* 2020, 11, 2342–2349.
- (33) You, C.; Liu, D.; Yu, J.; Tan, H.; Zhu, M.; Zhang, B.; Liu, Y.; Wang, Y.; Zhu, W. Boosting Efficiency of Near-Infrared Emitting Iridium(III) Phosphors by Administrating Their  $\pi-\pi$  Conjugation Effect of Core—Shell Structure in Solution-Processed OLEDs. *Adv. Opt. Mater.* **2020**, *8*, 2000154.
- (34) Caspar, J. V.; Meyer, T. J. Application of the Energy Gap Law to Nonradiative, Excited-State Decay. *J. Phys. Chem.* **1983**, 87, 952–957.
- (35) Freed, K. F.; Jortner, J. Multiphonon Processes in the Nonradiative Decay of Large Molecules. J. Chem. Phys. 1970, 52, 6272–6291.
- (36) Englman, R.; Jortner, J. The Energy Gap Law for Radiationless Transitions in Large Molecules. *Mol. Phys.* **1970**, *18*, 145–164.
- (37) Yersin, H. Triplet Emitters for Organic Light Emitting Diodes: Basic Properties. In *Highly efficient OLEDs with phosphorescent materials*; Yersin, H., Ed.; WILEY-VCH: Weinheim, 2008; pp. 1–97.
- (38) Yoon, S.; Teets, T. S. Red to Near-Infrared Phosphorescent Ir(III) Complexes with Electron-Rich Chelating Ligands. *Chem. Commun.* **2021**, *57*, 1975–1988.
- (39) Yoon, S.; Teets, T. S. Enhanced Deep Red to Near-Infrared (DR-NIR) Phosphorescence in Cyclometalated Iridium(III) Complexes. *Inorg. Chem. Front.* **2022**, *9*, 6544–6553.
- (40) Lai, P.-N.; Brysacz, C. H.; Alam, M. K.; Ayoub, N. A.; Gray, T. G.; Bao, J.; Teets, T. S. Highly Efficient Red-Emitting Bis-Cyclometalated Iridium Complexes. *J. Am. Chem. Soc.* **2018**, *140*, 10198–10207.
- (41) Kabir, E.; Wu, Y.; Sittel, S.; Nguyen, B.-L.; Teets, T. S. Improved Deep-Red Phosphorescence in Cyclometalated Iridium Complexes via Ancillary Ligand Modification. *Inorg. Chem. Front.* **2020**, *7*, 1362–1373.
- (42) Lai, P.-N.; Yoon, S.; Teets, T. S. Efficient Near-Infrared Luminescence from Bis-Cyclometalated Iridium(III) Complexes with Rigid Quinoline-Derived Ancillary Ligands. *Chem. Commun.* **2020**, *56*, 8754–8757.
- (43) Yersin, H.; Rausch, A. F.; Czerwieniec, R.; Hofbeck, T.; Fischer, T. The Triplet State of Organo-Transition Metal Compounds. Triplet Harvesting and Singlet Harvesting for Efficient OLEDs. *Coord. Chem. Rev.* 2011, 255, 2622–2652.
- (44) Espinoza, E. M.; Clark, J. A.; Soliman, J.; Derr, J. B.; Morales, M.; Vullev, V. I. Practical Aspects of Cyclic Voltammetry: How to Estimate Reduction Potentials When Irreversibility Prevails. *J. Electrochem. Soc.* **2019**, *166*, H3175—H3187.
- (45) Nonoyama, M. Benzo[h] Quinolin-10-yl-N Iridium(III) Complexes. Bull. Chem. Soc. Jpn. 1974, 47, 767–768.
- (46) Seybold, P. G.; Gouterman, M. Porphyrins: XIII: Fluorescence Spectra and Quantum Yields. *J. Mol. Spectrosc.* **1969**, *31*, 1–13.
- (47) Perdew, J. P.; Burke, K.; Ernzerhof, M. Generalized Gradient Approximation Made Simple. *Phys. Rev. Lett.* **1996**, *77*, 3865–3868.
- (48) Schäfer, A.; Huber, C.; Ahlrichs, R. Fully Optimized Contracted Gaussian Basis Sets of Triple Zeta Valence Quality for Atoms Li to Kr. *J. Chem. Phys.* **1994**, *100*, 5829–5835.
- (49) Schäfer, A.; Horn, H.; Ahlrichs, R. Fully Optimized Contracted Gaussian Basis Sets for Atoms Li to Kr. J. Chem. Phys. **1992**, 97, 2571–2577
- (50) Dolg, M.; Wedig, U.; Stoll, H.; Preuss, H. Energy-adjusted *Ab Initio* Pseudopotentials for the First Row Transition Elements. *J. Chem. Phys.* **1987**, *86*, 866–872.
- (51) Miertuš, S.; Scrocco, E.; Tomasi, J. Electrostatic Interaction of a Solute with a Continuum. A Direct Utilizaion of AB Initio Molecular Potentials for the Prevision of Solvent Effects. *Chem. Phys.* **1981**, *55*, 117–129.
- (52) Tomasi, J.; Mennucci, B.; Cammi, R. Quantum Mechanical Continuum Solvation Models. *Chem. Rev.* **2005**, *105*, 2999–3094.

- (53) Cancès, E.; Mennucci, B.; Tomasi, J. A New Integral Equation Formalism for the Polarizable Continuum Model: Theoretical Background and Applications to Isotropic and Anisotropic Dielectrics. *J. Chem. Phys.* **1997**, *107*, 3032–3041.
- (54) Mennucci, B.; Cancès, E.; Tomasi, J. Evaluation of Solvent Effects in Isotropic and Anisotropic Dielectrics and in Ionic Solutions with a Unified Integral Equation Method: Theoretical Bases, Computational Implementation, and Numerical Applications. *J. Phys. Chem. B* 1997, 101, 10506–10517.
- (55) Mulliken, R. S. Electronic Population Analysis on LCAO-MO Molecular Wave Functions. I. *J. Chem. Phys.* **1955**, 23, 1833–1840.
- (56) Reed, A. E.; Curtiss, L. A.; Weinhold, F. Intermolecular Interactions from a Natural Bond Orbital, Donor-Acceptor Viewpoint. *Chem. Rev.* **1988**, 88, 899–926.
- (57) Bachrach, S. M. Population Analysis and Electron Densities from Quantum Mechanics. In *Reviews in Computational Chemistry*; Lipkowitz, K. B., Boyd, D. B., Eds.; John Wiley & Sons, Inc.: Hoboken, NJ, USA, 2007; pp. 171–228, DOI: 10.1002/9780470125823.ch3.
- (58) Gorelsky, S. I. Quantitative Descriptors of Electronic Structure in the Framework of Molecular Orbital Theory. In *Advances in Inorganic Chemistry*; Elsevier, 2019; Vol. 73, pp. 191–219, DOI: 10.1016/bs.adioch.2018.12.001.
- (59) Gorelsky, S. I. AOMix: Program for Molecular Orbital Analysis; York University: Toronto, 1997. http://www.sg-chem.net. Accessed January 2018.
- (60) Gorelsky, S. I.; Lever, A. B. P. Electronic Structure and Spectra of Ruthenium Diimine Complexes by Density Functional Theory and INDO/S. Comparison of the Two Methods. *J. Organomet. Chem.* **2001**, 635, 187–196.
- (61) Frisch, M. J.; Trucks, G. W.; Schlegel, H. B.; Scuseria, G. E.; Robb, M. A.; Cheeseman, J. R.; Scalmani, G.; Barone, V.; Petersson, G. A.; Nakatsuji, H.; Li, X.; Caricato, M.; Marenich, A. V.; Bloino, J.; Janesko, B. G.; Gomperts, R.; Mennucci, B.; Hratchian, H. P.; Ortiz, J. V.; Izmaylov, A. F.; Sonnenberg, J. L.; Williams; Ding, F.; Lipparini, F.; Egidi, F.; Goings, J.; Peng, B.; Petrone, A.; Henderson, T.; Ranasinghe, D.; Zakrzewski, V. G.; Gao, J.; Rega, N.; Zheng, G.; Liang, W.; Hada, M.; Ehara, M.; Toyota, K.; Fukuda, R.; Hasegawa, J.; Ishida, M.; Nakajima, T.; Honda, Y.; Kitao, O.; Nakai, H.; Vreven, T.; Throssell, K.; Montgomery, J. A., Jr.; Peralta, J. E.; Ogliaro, F.; Bearpark, M. J.; Heyd, J. J.; Brothers, E. N.; Kudin, K. N.; Staroverov, V. N.; Keith, T. A.; Kobayashi, R.; Normand, J.; Raghavachari, K.; Rendell, A. P.; Burant, J. C.; Iyengar, S. S.; Tomasi, J.; Cossi, M.; Millam, J. M.; Klene, M.; Adamo, C.; Cammi, R.; Ochterski, J. W.; Martin, R. L.; Morokuma, K.; Farkas, O.; Foresman, J. B.; Fox, D. J. Gaussian 16 Rev. C.01, Gaussian Inc., 2016.